Seismic Velocity Prediction in Shallow (<30 m) Partially Saturated, Unconsolidated Sediments Using Effective Medium Theory

Jie Shen[1,*], James M. Crane[2], Juan M. Lorenzo[1] and Chris D. White[3]
[1]Department of Geology & Geophysics, Louisiana State University, E235 Howe Russell Kniffen, Baton Rouge, LA 70803
Email: bjshenjie@gmail.com
[2]Chevron Corporation, 2932 Johnston Street, Lafayette, LA 70503
[3]Department of Petroleum Geology, Louisiana State University, 142 Old Forestry, Baton Rouge, LA 70803

*Now at Shell Exploration & Production Company, 701 Poydras Street, New Orleans, LA 70139

ABSTRACT

Seismic velocity models of the near-surface (<30 m) better explain seismic velocities when all elements of total effective stress are considered, especially in materials with large cohesive and soil suction stress such as clays. Traditional constitutive elastic models that predict velocities in granular materials simplify the effect of total effective stress by equating it to net overburden stress, while excluding interparticle stresses and soil suction stress. A new proposed methodology calculates elastic moduli of granular matrices in near-surface environments by incorporating an updated definition of total effective stress into Hertz-Mindlin theory and calculates the elastic moduli of granular materials by extending Biot-Gassmann theory to include pressure effects induced by water saturation changes and cohesion. At shallow depths, when water saturation increases, theoretically calculated seismic velocities decrease in clay and increase in sand because interparticle stresses suppress the Biot-Gassmann effect. For standard sand and clay properties, net overburden stress becomes more influential than interparticle stresses at depths greater than 10 cm in sand and 100 m in clay. Pore pressure in the new model also incorporates the effect of layer thickness and pore size variation. Traditional calculation of pore pressure assumes a constant pore size medium, but may lead to an under- or overestimation of velocity by up to 20%. In clays, the variation of seismic velocity with water saturation is almost double the range predicted when only net overburden stress is considered to influence stress at the grain contacts. The proposed model predicts seismic velocities that compare well with measured field velocities from the literature.

Introduction

Currently, constitutive elastic models for granular materials are used to explain observed seismic velocities in sands (Bachrach *et al.*, 1998; Velea *et al.*, 2000) over shallow depths (<30 m). However, velocity predictions may show improvement when additional sources of interparticle stress are considered such as those caused by capillarity (Tinjum *et al.*, 1997) and cohesivity. These additional effects are especially significant in clay-rich soils. Through improved elastic models, observed seismic velocity can be inverted (Aster *et al.*, 2013; Eberhart-Phillips *et al.*, 1989) to better estimate parameters such as water saturation, porosity, matrix elastic moduli, or pressure.

The influences of pore content, matrix composition, and pressure on elasticity can be related through the elastic wave equation by implementing fluid substitution theory (Biot, 1956; Gassmann, 1951) and granular contact theory (Hertz, 1882; Mindlin, 1949). The Biot-Gassmann theory effectively explains the influence of pore constituent variations on elasticity and density of the porous media. When pore contents, such as water or air, have no shear resistance, the effective shear modulus is equal to the shear modulus of the granular matrix. In conventional Biot-Gassmann theory, elastic moduli of the granular matrix are considered constant. As water saturation increases in the pore space, a decrease in the seismic velocity is attributed to the Biot-Gassmann effect (Wulff and Burkhardt, 1997) because the bulk density increases more than the effective bulk modulus of the overall granular material.

Velocity predictions from Biot theory are frequency-dependent (Biot, 1956). When a seismic wave propagates

 DOI: 10.2113/JEEG21.2.67

through a fluid-filled porous medium at low frequencies (lower than critical frequency) (Mavko *et al.*, 2009), Biot theory assumes the fluids and matrix move in phase so only a small amount of energy dissipation occurs. The critical frequency (ω_c) defines the boundary between low and high frequencies in Biot theory: $\omega_c = \eta\Phi/\kappa\rho_f$, where η is viscosity, Φ is porosity, κ is permeability and ρ_f is fluid density (Mavko *et al.*, 2009). In this case, expressions derived from Biot theory are the same as those from Gassmann theory. When a wave propagates at high frequencies (higher than critical frequency) (Mavko *et al.*, 2009), Biot theory also predicts velocities of dissipative waves, which are caused by the fluid and matrix moving out of phase. In some dispersion cases where Biot theory is not applicable, workers have developed other theories to predict wave propagation with velocity dispersion and attenuation, such as squirt-flow mechanism (Mavko and Jizba, 1991; Mavko and Nur, 1979) and an integration of Biot and squirt-flow model (Dvorkin and Nur, 1993).

Hertz-Mindlin contact theory (Hertz, 1882; Mindlin, 1949) is used to calculate the elastic moduli of elastic granular materials in terms of porosity, grain contact geometry, grain elasticity, and grain contact stress. Hertz-Mindlin theory predicts that seismic velocity (V) will increase as a power function of stress (σ) ($V \propto \sqrt[6]{\sigma}$) (Mindlin, 1949). In conventional Hertz-Mindlin theory, net overburden stress (Eaton, 1969) is typically used to represent stress at the grain contacts.

Total effective stress represents the average stress carried by the granular matrix and was first defined as total stress minus pore pressure (Terzaghi, 1943). Today, the total effective stress is defined as the sum of net overburden stress and interparticle stresses (Bishop, 1960; Lu and Likos, 2006). Interparticle stresses contribute to the total effective stress and include capillary stress arising from the interfacial tension between grains and the wetting phase (Tinjum *et al.*, 1997), negative pore water pressure (Rinaldi and Casagli, 1999), and physicochemical stresses caused by van der Waals attractions, electrical double layer repulsion, and chemical cementation effects (Ikari and Kopf, 2011). Interparticle stresses can be classified into stresses in fully saturated media (σ_{co}), that confer cohesion to sediments, and stresses in unsaturated media that result as water saturation changes (σ'_s – soil suction stress) (Lu and Likos, 2006). Interparticle stresses are important in the near-surface (0–100 m) because they increase the pressure at grain contacts and can be several orders of magnitude (MPa) larger than the net overburden stress. Net overburden stress estimation can be difficult at depths near a changing water table, because the weight of sediment below the water table is effectively lowered by buoyancy (Turner, 1979). In this case, buoyancy is the displacement of water by sediments (Archimedes' Principle) and results in a decrease in total effective stress on the granular matrix and also the seismic velocity.

Several field studies demonstrate that both net overburden stress and interparticle stresses, particularly in shallow unconsolidated sediments, are important to consider when developing constitutive elastic models. However, interparticle stresses have yet to be included in constitutive elastic models for predicting seismic velocity of granular material (Dvorkin *et al.*, 1999). In shallow unconsolidated sediments, seismic velocities can be underestimated if interparticle stresses are excluded when calculating pressure at grain contacts. Lu and Sabatier (2009) document water saturation, temperature, stress, and compressional velocity in shallow soil over a two year period. The range in measured velocities (260–460 m/s) cannot be predicted by changes in net overburden stress (<5 kPa) and must also include changes in interparticle stresses (>350 kPa). In traditional elastic models, the exclusion of interparticle stresses for the case of deep, unconsolidated sediments remains valid where net overburden stresses are several orders of magnitude more than interparticle stresses (Dvorkin and Nur, 1996).

We propose a constitutive elastic model, suitable for use in unconsolidated clay as well as sand, that estimates elastic moduli of elastic granular materials by extending conventional Hertz-Mindlin and Biot-Gassmann theories to incorporate interparticle stresses. An updated definition of total effective stress that includes interparticle stresses is incorporated into Hertz-Mindlin theory. Because total effective stress changes with water saturation, the bulk modulus and shear modulus of the granular matrix (K_{matrix} and G_{matrix}, respectively) vary throughout the full range of saturations. The elastic moduli of the granular matrix increase as the net overburden stress increases with depth and vary with interparticle stresses as water saturations change. Traditionally, Biot-Gassmann theory estimates elastic properties of granular materials by varying the elastic properties of the pore space as the pore constituents change in concentration, but assumes that the elastic properties of the granular matrix are constant. However, Biot-Gassmann theory can also account for changes in the elastic properties of the granular matrix during changes in water saturation by updating the reference elastic moduli of the matrix through Hertz-Mindlin theory.

The influence of interparticle stresses is demonstrated by calculating theoretical seismic velocities from physical properties of sand and clay (Table 1) with varied total effective stresses and water saturations. Our modeled velocities are indistinguishable from those calculated from traditional Hertz-Mindlin and Biot-Gassmann

Table 1. Physical and theoretical properties and model parameters of sands and clays for seismic velocity calculations. van Genuchten parameters (van Genuchten, 1980) are calibrated for capillary pressures in sands (psi) and clays (kPa).

Model parameters	Sand	Reference	Clay	Reference
Grain Shear Modulus (Pa)	4.5×10^{10}	Mavko *et al.* (2009)	9.9×10^{9}	Mavko *et al.* (2009)
Grain Bulk Modulus (Pa)	3.66×10^{10}		2.5×10^{10}	
Grain Density (kg/m^3)	2,650		2,550	
Grain Poisson's Ratio	0.15		0.15	
Porosity	0.35		0.56	
Water Density (kg/m^3)	1,000		1,000	
Air Density (kg/m^3)	1.22		1.22	
Gravitational Acceleration (m/s^2)	9.81		9.81	
Coordination Number	1		1	
van Genuchten n Fitting Parameter	5.69	Engel *et al.* (2005)	2	Song *et al.* (2012)
van Genuchten α Fitting Parameter (1/m)	4.56		0.01	
Irreducible Water Content	0.024		0.10	
Matrix Cohesion (Pa)	300	Krantz (1991)	16,000	Bishop (1960)

methodologies at large confining pressures (>5 MPa) and low interparticle stresses (<2 kPa); however, calculated seismic velocities for materials with large interparticle stresses can be very different. Calculated seismic velocities are also compared successfully to measured field velocities (Lu and Sabatier, 2009) obtained at small confining pressures (<5 kPa) and over a large total effective stress range (>350 kPa) to validate the new model.

Theory

Seismic velocities are related to the effective moduli and density of media (*e.g.*, Ikelle and Amundsen, 2005):

$$V_P = \sqrt{\frac{K_{eff}+\frac{4}{3}G_{eff}}{\rho_{bulk}}} \tag{1}$$

$$V_S = \sqrt{\frac{G_{eff}}{\rho_{bulk}}}, \tag{2}$$

where V_P is the P-wave velocity, V_S is the S-wave velocity, K_{eff} is the effective bulk modulus, G_{eff} is the effective shear modulus, and ρ_{bulk} is the bulk density. The "*eff*" subscript is used to differentiate the elastic moduli of the bulk granular material from the elastic moduli of the granular matrix, pore space, or individual grains.

In Eqs. (1) and (2), bulk density is the weighted mean of matrix and pore space densities. When the pore space is filled by a combination of water and air, the equation for bulk density becomes (Bourbie *et al.*, 1992):

$$\rho_{bulk} = \phi(S_w\rho_{water}+(1-S_w)\rho_{air})+(1-\phi)\rho_{grain}, \tag{3}$$

where Φ is the porosity of the skeletal matrix, S_w is the water saturation, ρ_{water} is the density of water, ρ_{air} is the density of air, and ρ_{grain} is the grain density. Bulk density is needed for input into the elastic wave equation.

Biot-Gassmann theory (Biot, 1956; Gassmann, 1951) effectively explains the influence of pore constituent variations on elasticity and density of the porous media. The bulk modulus of the pore space is a weighted harmonic mean of the bulk moduli of the pore constituents. When pore contents such as water or air have no shear resistance, the effective shear modulus is equal to the shear modulus of the granular matrix. Biot-Gassmann theory is implemented to calculate the effective bulk moduli and shear moduli (Eqs. (1) and (2)) for granular materials (mixture of grains, gas, and fluid) from the elastic moduli of the matrix (Mavko *et al.*, 2009):

$$\frac{K_{eff}}{K_0-K_{eff}} = \frac{K_{matrix}}{K_0-K_{matrix}}+\frac{K_{pore}}{\phi\left(K_0-K_{pore}\right)} \tag{4}$$

$$G_{eff} = G_{matrix}, \tag{5}$$

where K_0 is the bulk modulus of the grains and K_{pore} is the bulk modulus of the pore space.

When the two pore constituents are water and air, the bulk modulus of the pore space (K_{pore}) (Eq. (4)) can be calculated (Mavko *et al.*, 2009):

$$\frac{1}{K_{pore}} = \frac{S_w}{K_{water}}+\frac{1-S_w}{K_{air}}, \tag{6}$$

where S_w is water saturation, K_{water} is the bulk modulus of water, and K_{air} is the bulk modulus of air. In conventional Biot-Gassmann theory, elastic moduli of the granular matrix are considered to be constant. Note that variables with a "matrix" subscript are used instead of the "dry" subscript used in conventional Biot-Gassmann fluid substitution equations (Bachrach *et al.*, 1998). The new notation is used to better show that we are using a reference matrix elasticity, whether wet or dry. In unconsolidated sediments G_{eff} is equal to G_{matrix} at a particular depth and water saturation, but neither is constant throughout the full range of saturations. The depth and water saturation dependence of matrix elasticity is due to total effective stress contributions of net overburden stress and soil suction stress, respectively.

Matrix elastic moduli (Eqs. (4) and (5)) are calculated by Hertz-Mindlin theory (Hertz, 1882; Mindlin, 1949). Unlike the conventional Hertz-Mindlin theory, which only considers net overburden stress as effective stress, we incorporate both interparticle stresses (soil suction and cohesive stress) and overburden stress in the total effective stress P of our new model (Mavko *et al.*, 2009):

$$K_{matrix} = \sqrt[3]{\frac{n^2(1-\Phi)^2 G^2}{18\pi^2(1-\nu)^2} P} \tag{7}$$

$$G_{matrix} = \frac{5-4\nu}{5(2-\nu)} \sqrt[3]{\frac{3n^2(1-\Phi)^2 G^2}{2\pi^2(1-\nu)^2} P}, \tag{8}$$

where n is grain coordination number, G is the grain shear modulus, ν is the grain Poisson's ratio, K_{matrix} is the bulk modulus of the skeletal matrix, G_{matrix} is the shear modulus of the skeletal matrix, and P is the total effective stress.

Total effective stress at the grain contacts is used to calculate matrix elasticity in Hertz-Mindlin theory (Eqs. (7) and (8)). In the absence of direct measurements, total effective stress can be estimated from the sum of net overburden stress ($\sigma_t - u_{pore}$) and interparticle stress ($\sigma'_s + \sigma_{co}$) acting on the granular matrix (Lu and Likos, 2006):

$$P = (\sigma_t - u_{pore}) + \sigma'_s + \sigma_{co}, \tag{9}$$

where σ_t is the total external stress, u_{pore} is pore pressure, σ'_s is soil suction stress (Lu and Likos, 2006), and σ_{co} is apparent tensile stress at the saturated state caused by cohesive or physicochemical forces (Bishop, 1960). Soil suction is calculated from van Genuchten fitting parameters and water saturation (Song *et al.*, 2012). Saturated cohesion is constant for different soil types and is taken from the literature (Table 1).

The soil water characteristic curve (SWCC), relating suction stress and water content, is useful if water saturations need to be estimated above a given water table. SWCCs are expected to display hysteresis, which is a difference in suction stress between the wetting and draining stages because of the hydrophilic nature of soils. A SWCC can be converted into a pressure head–water saturation profile by solving Eq. (9) for capillary pressure ($u_a - u_w$) and setting it equal to the weight of the water column supported above the water table (pore pressure equation). The pressure head can then be plotted against water saturation, creating a pressure head-water saturation profile. The work of van Genuchten (1980) is used to empirically fit capillary pressures and water saturations for different sediments:

$$S_e = \frac{\theta - \theta_r}{\theta_s - \theta_r} = \left[\frac{1}{1+[\alpha(u_a - u_w)]^n}\right]^{\frac{n-1}{n}}, \tag{10}$$

where S_e is effective saturation, θ is the volumetric water content, θ_r is the residual water content, θ_s is the saturated water content, which is equivalent to porosity, α and n are van Genuchten (1980) empirical fitting parameters, and ($u_a - u_w$) is capillary pressure.

Soil suction stress (Eq. (9)) is then derived from the van Genuchten's fitting parameters for SWCC (Song *et al.*, 2012):

$$\sigma'_s = -\frac{S_e}{\alpha}\left(S_e^{\frac{n}{1-n}} - 1\right)^{\frac{1}{n}}. \tag{11}$$

Pore Pressure in Homogeneous Soils

For the derivation of pore pressure, we assume homogeneous soils can be represented by a medium with a constant pore size and no layering (Figs. 1(a) and (c)). The difference in the calculation of pore pressure (Eq. (9)) can be up to 20% between that for a single pore size medium (Figs. 1(a) and (c)) and a layered soil medium (Figs. 1(b) and (d)).

In homogeneous soils, pore pressure (u_{pore}) is simply calculated from the weight of the water column (Fredlund and Rahardjo, 1993):

$$u_{pore} = \rho_{water} g h_b, \tag{12}$$

where ρ_{water} is the density of water, g is gravitational acceleration, and h_b is the height of the sediment column supported by buoyancy.

If normal stress from the weight of the sediment is much larger than horizontal stresses, the difference ($\sigma_t - u_{pore}$) becomes the net overburden stress and is the weight of the sediment above the grain contact minus the local pore pressure (Terzaghi, 1943):

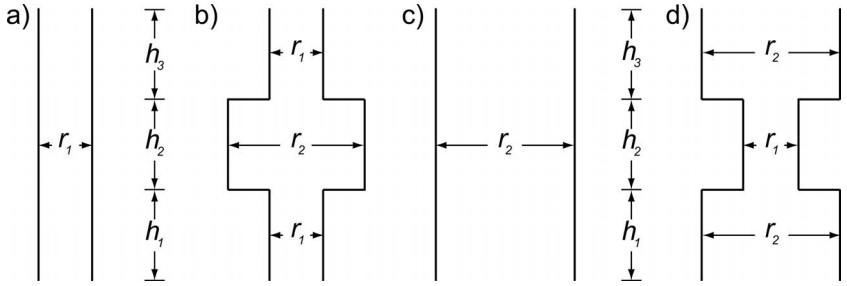

Figure 1. Simplified pore size model used to calculate matric suction in three-layer soils. a) A single, narrow pore size (r_1) occurs when the 3 layers (h_1+h_2+h_3) consist of homogeneous clay. b) If the middle layer contains sand, the pore size is larger (r_2). c) A single, thick pore size (r_2) occurs when the 3 layers (h_1+h_2+h_3) consist of homogeneous sand. d) When the middle layer contains clay (r_1) sandwiched between sand (r_2), the narrowest pore size is in the center.

$$\begin{aligned} \textit{Net overburden stress} &= \sigma_t - u_{pore} \\ &= \rho_{bulk} g h_a + (\rho_{bulk} - \rho_{water}) g h_b, \end{aligned} \quad (13)$$

where h_a is the height of the sediment column not influenced by buoyancy.

Pore Pressure in a Clay-Sand-Clay Three-Layer Soil

In variable pore size layered soils that are not dominated by one type of soil, we examine the effects of a pore size change with a simple, three-layered soil using capillary tubes with various radii to conceptualize the calculations. Natural soils often have layers of alternating sand and clay composition. Usually, pore size in clay is smaller than in sand as the grain size of clay is smaller than sand (Taylor, 1948). We can simplify more complicated field conditions by considering two idealized cases: one case where sand is sandwiched between clay layers (Fig. 1(b)) and another for clay sandwiched between sand layers (Fig. 1(d)). A three-layer pore size model (Fig. 1) that attempts to mimic a clay-sand-clay alternation has the thickest pore size in the middle layer. Pore pressure estimates are the same for the bottom layer in both pore size models (Eq. 12), but different in both cases within top and middle layers (Figs. 1(b) and (d)).

In layered soil, pore pressure (u_{pore}) is equal to the total stress difference at the air-water interface and depends on layer thickness, pore-size variation and capillary head height. To simplify the derivation, we use a capillary tube to represent idealized pore size in soil (Fig. 1). In equilibrium, pore pressure around a capillary tube is balanced by the weight of the water column pulled up by surface tension (Fredlund and Rahardjo, 1993). Three cases arise depending on the location of the capillary head within the three layers:

Case 1: When the capillary head (h_c) is within the bottom clay layer ($h_c < h_1$), pore pressure u_{pore1} can be estimated by the weight of the water column using Eq. (12).

Case 2: When the capillary head (h_{c2}) rises into the middle sand layer ($h_1 < h_{c2} < h_1 + h_2$), pore pressure u_{pore2} can be calculated as:

$$u_{pore2} = \left(\frac{r_1}{r_2}\right)^2 \rho_w g h_{c2} + \left(1 - \frac{{r_1}^2}{{r_2}^2}\right) \rho_w g (h_{c2} - h_1), \quad (14)$$

where r_1 and r_2 are narrow and thick pore sizes occurring in clay and sand, respectively. As the pore pressure is less in the middle layer than in the bottom layer, water will tend to stay in the bottom thin-throat layer longer before it eventually rises up into the second layer (Taylor, 1948).

Case 3: When the capillary head (h_{c3}) rises and enters the top clay layer ($h_2 < h_{c3} < h_1 + h_2 + h_3$), pore pressure u_{pore3} becomes:

$$u_{pore3} = \rho_w g h_{c3} + \left(\frac{{r_2}^2}{{r_1}^2} - 1\right) \rho_w g h_2, \quad (15)$$

Pore pressure can be misestimated if the pore pressure calculation assumes only one homogeneous layer with a constant pore size for clay-sand-clay layered soils, such as in case 2, where pore pressure is overestimated, and in case 3, where pore pressure is underestimated.

Pore Pressure in a Sand-Clay-Sand Three-Layer Soil

Pore pressure may also be estimated for the case of a three-layer pore size model (Fig. 1(d)) that attempts to mimic a sand-clay-sand alternation that has the narrowest pore size in the middle layer. We consider three cases:

Case 1: When the capillary head (h'_c) is within the bottom sand layer ($h'_c < h_1$), pore pressure u'_{pore1} can be estimated by the weight of the water column using Eq. (12).

Case 2: When the capillary head (h'_{c2}) rises into the middle clay layer ($h_1 < h'_{c2} < h_1 + h_2$), pore pressure u'_{pore2} can be calculated as:

$$u'_{pore2} = \left(\frac{r_2}{r_1}\right)^2 \rho_w g h_1 + \rho_w g (h'_{c2} - h_1). \quad (16)$$

Case 3: When the capillary head (h'_{c3}) rises and enters the top sand layer ($h_2 < h'_{c3} < h_1 + h_2 + h_3$), pore pressure u'_{pore3} becomes:

$$u'_{pore3} = \frac{{r_1}^2}{{r_2}^2} \rho_w g h_2 + \rho_w g \left(h'_{c3} - h_2\right). \quad (17)$$

Pore pressure can be misestimated if the pore pressure calculation assumes only one homogeneous layer with a constant pore size for sand-clay-sand layered soils, such as in case 2, pore pressure is underestimated, and in case 3, pore pressure is overestimated. To properly use our proposed model to match field data in layered soils, it is necessary to incorporate the effect of layer thickness and pore size variation.

Theoretical Cases

In this section, we present several theoretical examples by assigning published values to parameters (Table 1) in the calculation of stresses and velocities, to illustrate the differences between traditional models and our proposed model. As sand and clay are common unconsolidated sediments, the parameters used to calculate theoretical results are for homogenous sand and clay soils. The variation of these properties is less than 5% for sand, but may vary up to 20% for clay (Mavko *et al.*, 2009). To simplify our examples, we choose one set of parameter values for sand and clay to represent typical trends of theoretical velocities or stresses. Different soil property values may result in as much as 10% change in calculated velocities for clay and less than 3% change for sand. Unrealistically low coordination numbers (= 1, Table 1) have been previously used to match low seismic velocities in shallow sediments by taking into account the angular grain shape, which is contrary to the assumption of spherical contact in Hertz-Mindlin theory (Bachrach *et al.*, 1998; Velea *et al.*, 2000). The low coordination numbers can lower the calculated velocity, but do not affect general velocity trends.

Our new model (Eqs. (9) and (11)) predicts that when water saturation changes, only soil suction stress contributes to the variation in total effective stress (Fig. 2). Among the three stress terms in the calculation of total effective stress (Eq. (9)), only soil suction stress is a function of effective water saturation (Eq. (11)). Both overburden and cohesion are not affected by saturation changes.

To highlight the influence of interparticle stresses on seismic velocity, we calculate velocities using either total effective stress (new model) or solely net overburden

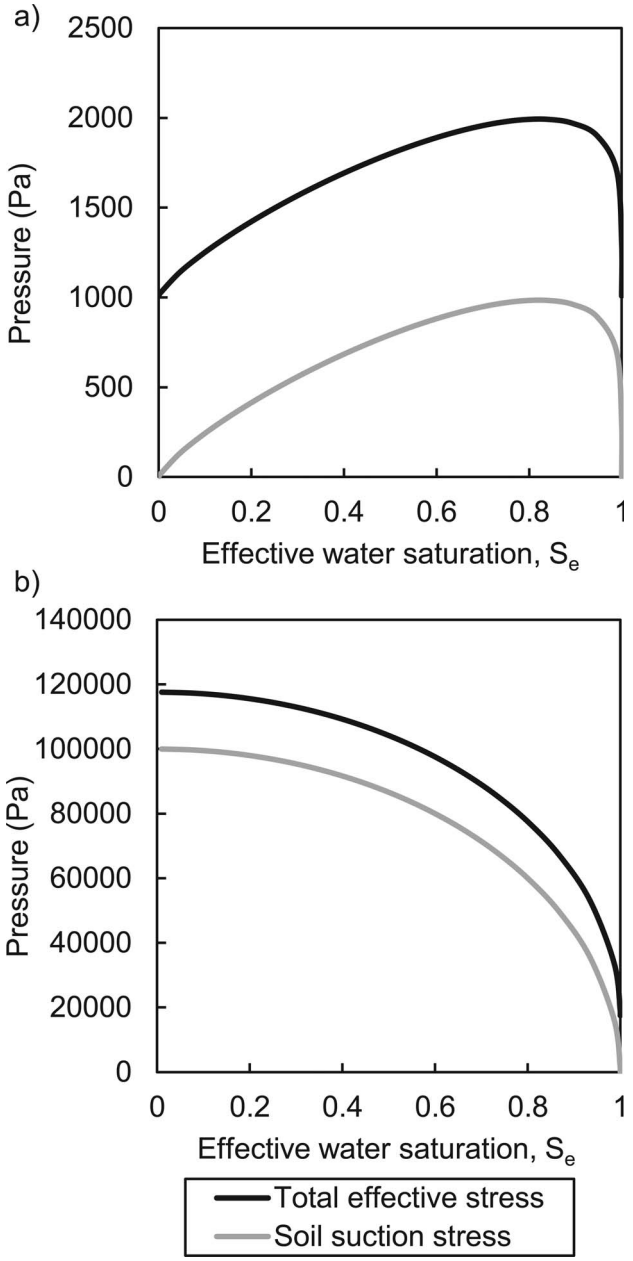

Figure 2. Contribution of soil suction stress to total effective stress as a function of effective water saturation for a) sand at 10-cm depth and b) clay at 1-m depth. The difference between the soil suction stress curve and the total effective stress curve is attributed to net overburden stress and cohesion, which remain constant throughout saturation changes.

stress (traditional model) at constant depths in different soils (Fig. 3). As the difference in velocity relies on the changes in stress and water saturation, they are the only variables that change within each example. We focus on using water saturation values greater than 10%, which are above residual water saturation, and less than 95%

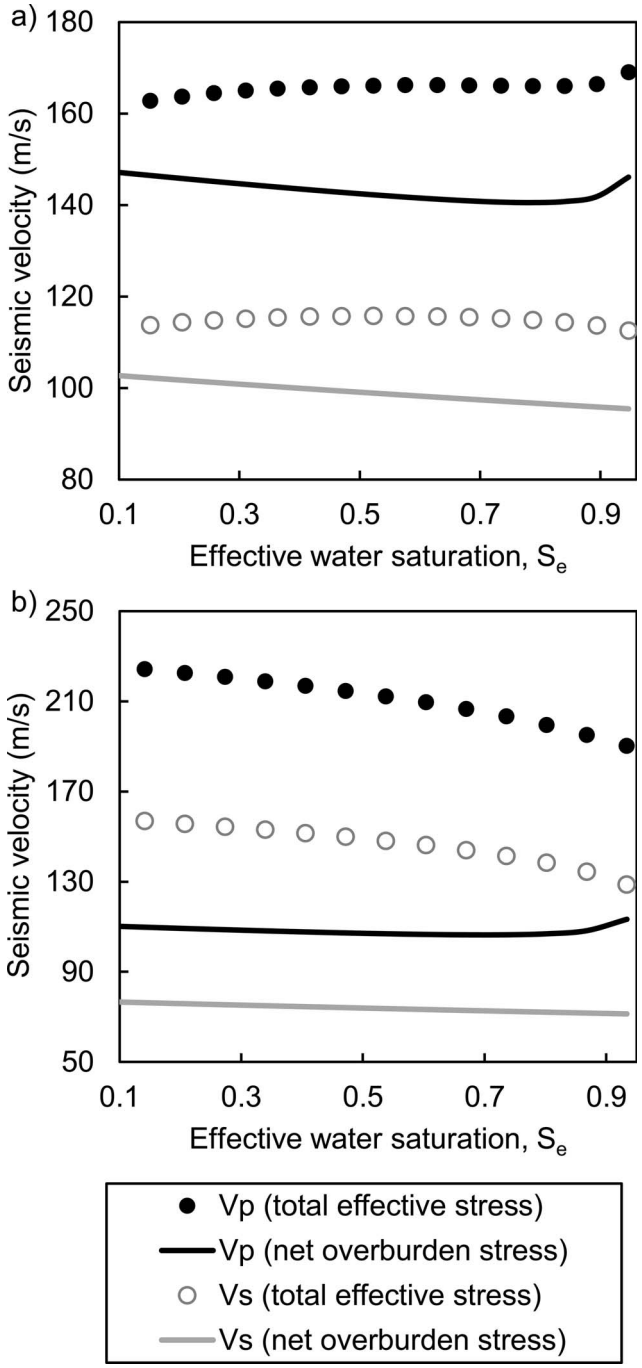

Figure 3. Compressional (V_P) and shear-wave (V_S) velocities are calculated for a) sand at 10-cm depth and b) clay at 1-m depth. The different trends in V_P and V_S from incorporating total effective stress (dots) and only net overburden stress (lines) are attributed to interparticle stresses.

because compressional seismic velocities can increase by over 10^3 m/s as water saturation approaches 100%. Normally, shallow soils are not fully saturated and observed velocities are on the order of 10^2 m/s. We also focus on this range of water saturations because interparticle stresses increase above a base value within this range. Above 95% water saturation, soil suction stress becomes negligible.

Field velocity profiles are sometimes depth-dependent, so we need to relate water saturation to depth for the prediction of field velocity. In our proposed model, we estimate the relationship between water saturation and depth from SWCCs (Fig. 4). Pressure head–water saturation profiles converted from capillary pressure–water saturation curves (*e.g.*, SWCC) are consistent with natural water saturation profiles (Desbarats, 1995). In the calculation of total effective stress (Eqs. (9), (11) and (13)), both net overburden stress and soil suction stress are depth-dependent. When depth changes, net overburden stress and soil suction stresses both contribute to the variation in sand and clay (Fig. 5). Velocity–depth profiles (Fig. 6) are calculated for sands and clays with stationary water tables to illustrate the decreasing effect of interparticle stresses as depth and net overburden stress increase.

Verification with Field Measurements

To verify our proposed model, we compare our predictions to observed field velocities (Lu and Sabatier, 2009) (Fig. 7). The uncertainty in soil property parameters (Table 1) and measured total effective stress (Lu and Sabatier, 2009) lead to less than $\pm 5\%$ error in predicted velocity. The majority of field velocities also fall within 5% of the predicted velocity range from our proposed model.

A traditional model fails to predict the variation in the observed field velocities from ~250 to ~450 m/s (Fig. 7). Without interparticle stresses (traditional model) contributing to grain contact stress, we would expect pore constituent concentrations to be the main variables affecting seismic velocity. However, changes in the bulk modulus and density of the pore space only account for an ~14 m/s increase in seismic velocity. The results (Fig. 7) indicate large interparticle stresses (up to 20 kPa) are much more influential on shallow seismic velocities (<30 cm) than net overburden stress or pore constituent concentrations.

Field velocity predictions require reasonable estimations of water saturation and total effective stress, both of which can be achieved from field measurements or estimated by our proposed model (using SWCC). For the velocity prediction in Fig. 7, total effective stress and water saturation are from field measurements (Lu and Sabatier, 2009). Total effective stress is input for the range of observed stresses. Total effective stress and water saturation measurements are highly variable so we simplify water saturation input

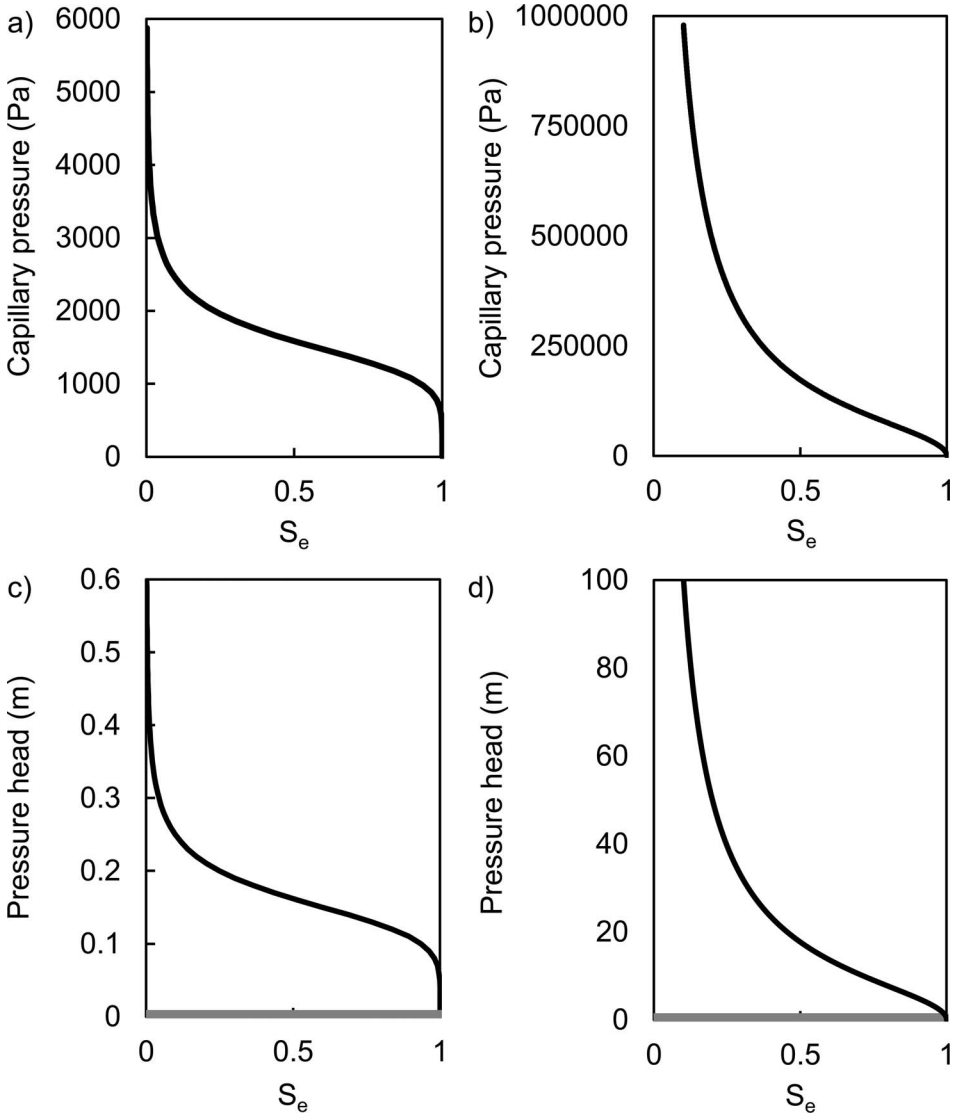

Figure 4. Soil-water characteristic curves for a) sand and b) clay calculated from van Genuchten fitting parameters (Table 1). The capillary pressures are converted to pressure head for input into velocity-depth models for c) sand and d) clay. The water tables are at 0-m pressure head.

by correlating several water saturation and total effective stress values from the raw data. Water saturation is highest (53%) at the lowest effective stress and is assumed to decrease linearly until it reaches its lowest value (10%) at the largest effective stress. This relationship appears to hold true ($\pm 2\%$ S_w) for the presented measurements. Total effective stress correlates with water saturation because of soil suction stress. The increase in velocity caused solely by changes in bulk modulus and density of the pore space is compared to measured velocities to further illustrate that interparticle stresses must be included in velocity calculations.

Discussion

In our proposed model, soil suction stress plays a more significant role in clay than in sand (Fig. 2). In sands, soil suction stress contributes to less than 50% of total effective stress, while overburden stress is the dominant stress at most saturation values (Fig. 2(a)). In clays, soil suction stress contributes to ~80% of total effective stress, except when the effective water saturation reaches 100% (where soil suction stress is 0) (Fig. 2(b)). At shallow depths (0–100 m), clays and sands may have different seismic velocity trends with water saturation because of their respective interparticle stresses.

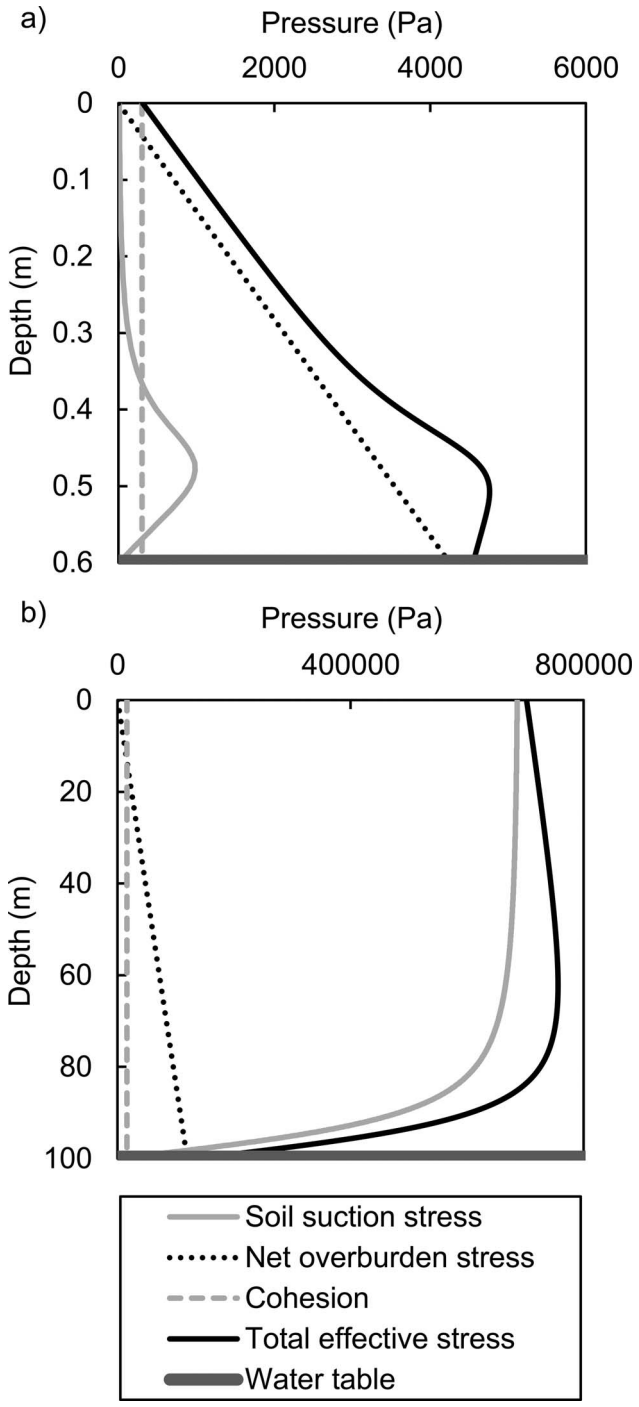

Figure 5. Contributions of soil suction stress, net overburden stress and cohesion to the calculation of total effective stress as a function of depth for a) sand when the water table is at a depth of 0.6 m and b) clay when the water table is at a depth of 100 m. The water table line (phreatic surface) shows where the pressure head is equal to atmospheric pressure. Saturation at each depth is calculated from fitting parameters of soil water characteristic curve (Table 1).

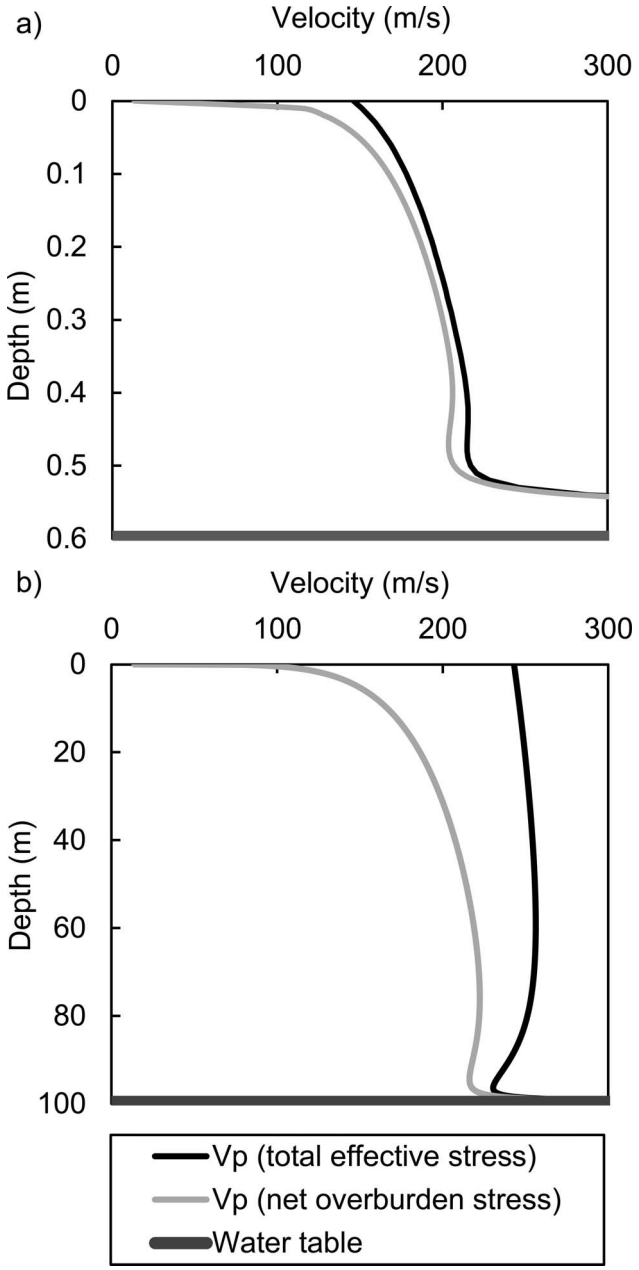

Figure 6. Seismic compressional wave velocities (V_P) calculated by incorporating total effective stress (black) or only net overburden stress (grey) for a) sand when the water table is at a depth of 0.6 m and b) clay when the water table is at a depth of 100 m. Saturation at each depth is input into the model, calculated from soil parameters (Table 1).

When interparticle stresses are included in our new model, there are significant differences in both values and trends of predicted seismic velocities from traditional models (Fig. 3). When total effective stress is used to calculate pressure instead of only net overburden stress, theoretical seismic velocities can be up to 20% higher in

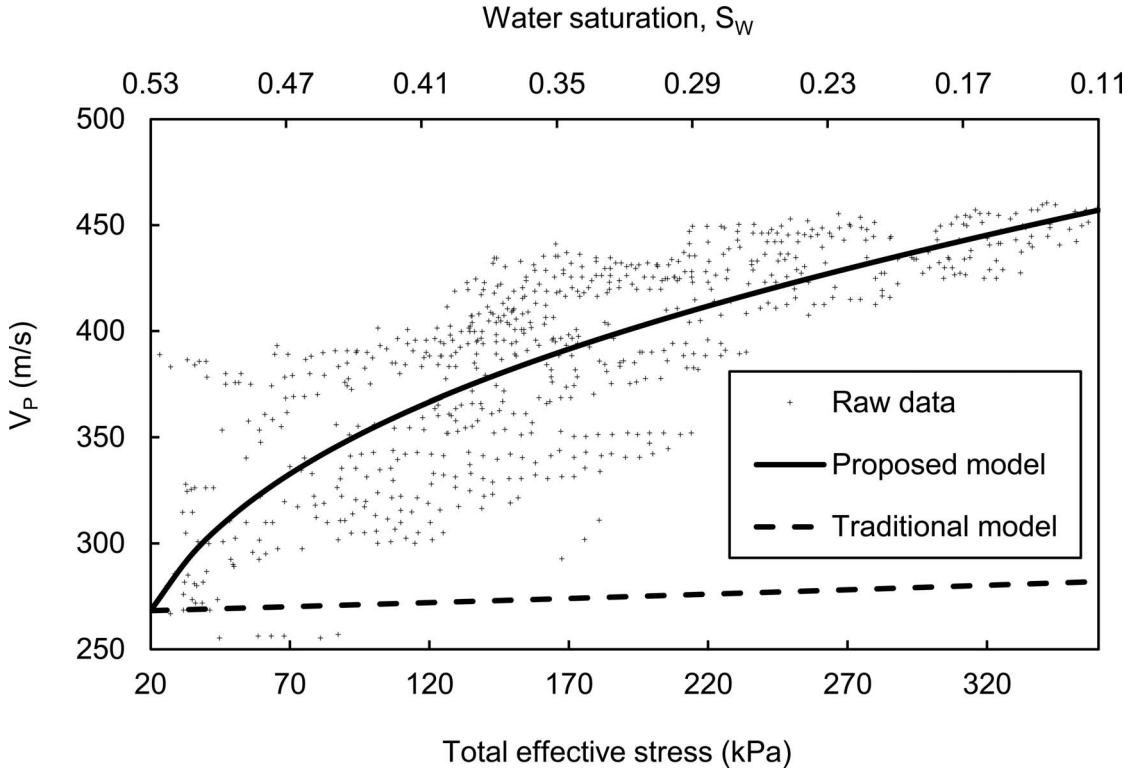

Figure 7. A comparison of raw data (Lu and Sabatier, 2009) (crosses) and predicted velocities from our proposed model (solid line) and a traditional model (dashed line). Model input parameters are for clay (Table 1) with the exception of coordination number, which is changed to 4.4 to provide the best fit to the data. The error in calculated velocities is less than $\pm 5\%$.

sands and up to 60% higher in clays. In sand, over a range of 10–95% water saturation, the predicted seismic velocity increases with water saturation and the Biot-Gassmann effect is not apparent (Fig. 3(a)). In clays, velocity decreases as water saturation increases, but when interparticle stresses are considered (new model) the calculated velocities double the range predicted by a traditional model (Fig. 3(b)). In comparison to sand, clay shows a larger variation in predicted velocities with changes in water saturation (Fig. 3). This greater sensitivity of velocity to water saturation makes clays more suitable for water saturation modeling.

Some water table monitoring studies attribute a decrease in velocity to lowered water tables because of the Biot-Gassmann effect (Bachrach *et al.*, 1998; Birkelo *et al.*, 1987). However, calculations of seismic velocity that include interparticle stresses (new model) predict an increase in seismic velocity with increasing water saturation in sand (Fig. 3(a)), so that a lower seismic velocity may not be attributed solely to the Biot-Gassmann effect. Instead, a decrease in velocity may be caused by buoyancy. In normally-pressured sands, the net overburden stress gradient can decrease up to ~9,800 Pa/m with the addition of water because of buoyancy. Thus, because of the decrease in the net overburden stress gradient, seismic velocities will decrease ($V\alpha\sqrt[6]{\sigma}$).

In our proposed model, the relative contributions of net overburden, soil suction and cohesive stresses to total effective stress depends on both depth and soil types (Fig. 5). In sands, net overburden stress is the dominant stress except just below the surface (<5-cm depth). Also in sand, a local maximum arises in total effective stress just above the water table (~50-cm depth) and it is attributed to the effect of soil suction stress. In clay, interparticle stresses (soil suction and cohesive stresses) dominate total effective stress until the water table is reached. Just above the water table, the sum of net overburden and soil suction stresses leads to a local maximum in total effective stress (~80-m depth) in clays. At the water table for both sand and clay, soil suction stress becomes 0 and the total effective stress becomes the sum of net overburden stress and cohesion. For example, in our case, net overburden stress equals the value of interparticle stresses at ~5 cm in sand and ~98 m in clay (Fig. 5).

Velocity–depth profiles calculated using either total effective stress (as in our new model) or only net overburden stress (as in a traditional model) are most different at the surface, but converge near the water table (Fig. 6).

Calculated velocities have similar trends as depth increases and net overburden stress becomes the largest component of total effective stress. The minimum in velocity above the water table in both sands and clays is a result from the maximum in total effective stress (Figs. 5 and 6).

Interparticle stresses should be included in seismic velocity modeling of shallow unconsolidated sediments, even in sands, which have very low capillary pressures and cohesion, but especially in clays, which have very high interparticle forces. The large velocity variations measured by Lu and Sabatier (2009) at constant depths are better explained by interparticle stresses than density and elasticity changes during fluid substitution—these can only account for an ~8% velocity change (Fig. 6). When predicting seismic velocities, interparticle stresses are particularly important at depths less than 1 m in sands and 100 m in clays. At these depths, net overburden stress becomes a larger component of total effective stress than interparticle stresses. The proposed model remains applicable at large depths (>1 km) where our calculated velocities at large net overburden stresses (>5 MPa) are indistinguishable from previous models (Dvorkin and Nur, 1996).

Total effective stress is a required parameter in the proposed model. In the absence of direct measurements, total effective stress can be estimated from the SWCC, but specific temperature–pressure and wetting/drying conditions must be considered. Hysteresis in the SWCC for clays during wetting and drying cycles accounts for as much as 30% differences in capillary pressures and is attributed to a change in contact angle between the wetting phase and the solid surface (Pham *et al.*, 2005). Capillary pressure decreases by 3 kPa in sands as temperature increases from 20 to 80°C (She and Sleep, 1998). Our proposed model indicates that the total effective stress can also be estimated by considering the effect of pore-size variation and layer thickness in clay and sand layered soils.

Conclusions

An improvement in our understanding of total effective stress (Lu and Likos, 2006) in constitutive elastic models allows improved predictions of seismic velocity in both shallow sands and clays. The added effect of interparticle stresses suppresses the Biot-Gassmann effect in shallow sediments. When interparticle stresses are included, as water saturation increases, the decrease in seismic velocity can be two-times greater than that with traditional models. A greater change in seismic velocity implies that water saturation can be modeled with more accuracy in shallow clays than in sands. At depths greater than 10 cm in sands and 100 m in clays, net overburden stress becomes a larger component of total effective stress than interparticle stresses in the modeled granular materials. The proposed model predicts seismic velocities that fit well with field measured seismic velocities under low confining pressures (<5 kPa) and a large range of interparticle stresses (>350 kPa).

Acknowledgements

This work is supported by a Shell Exploration & Production Company Grant (2011–2015). We would like to thank the following for their support with scholarships and graduate assistantship to the first author: Geometrics Inc. Student Travel Grant for SAGEEP, Donald Towse Memorial Fund awarded by AAPG Grant-in-Aid, EnCana Scholarship, Imagine Resources Scholarship, H.V. Anderson Scholarship awarded by LSU Department of Geology and Geophysics, and especially to LSU Department of Geology and Geophysics for their active support of graduate student research.

References

Aster, R.C., Borchers, B., and Thurber, C.H., 2013, Parameter estimation and inverse problems: Academic Press, New York.

Bachrach, R., Dvorkin, J., and Nur, A., 1998, High-resolution shallow-seismic experiments in sand. Part 2: Velocities in shallow unconsolidated sand: Geophysics, **63**, 1234–1240.

Biot, M.A., 1956, Theory of propagation of elastic waves in a fluid - saturated porous solid. I. Low-frequency range: The Journal of the Acoustical Society of America, **28**, 168–178.

Birkelo, B.A., Steeples, D.W., Miller, R.D., and Sophocleous, M., 1987, Seismic reflection study of a shallow aquifer during a pumping test: Ground Water, **25**, 703–709.

Bishop, A.W., 1960, The principles of effective stress: Norges Geotekniske Institutt.

Bourbie, T., Coussy, O., Zinszner, B., and Junger, M.C., 1992, Acoustics of porous media: J. Acoustical Society of America, **91**, 3080.

Desbarats, A., 1995, Upscaling capillary pressure-saturation curves in heterogeneous porous media: Water Resources Research, **31**, 281–288.

Digby, P.J., 1981, The effective elastic moduli of porous granular rocks: Journal of Applied Mechanics, **48**, 803–808.

Dvorkin, J., and Nur, A., 1993, Dynamic poroelasticity; a unified model with the squirt and the Biot mechanisms: Geophysics, **58**, 524–533.

Dvorkin, J., and Nur, A., 1996, Elasticity of high-porosity sandstones: Theory for two North Sea data sets: Geophysics, **61**, 1363–1370.

Dvorkin, J., Prasad, M., Sakai, A., and Lavoie, D., 1999, Elasticity of marine sediments: Rock physics modeling: Geophysical Research Letters, **26**, 1781–1784.

Eaton, B., 1969, Fracture gradient prediction and its application in oilfield operations: Journal of Petroleum Technology, **21**, 1353–1360.

Eberhart-Phillips, D., Han, D.H., and Zoback, M.D., 1989, Empirical relationships among seismic velocity, effective pressure, porosity, and clay content in sandstone: Geophysics, **54**, 82–89.

Engel, J., Schanz, T., and Lauer, C., 2005, State parameters for unsaturated soils, basic empirical concepts: Springer, Berlin Heidelberg, 125–138.

Fredlund, D.G., and Rahardjo, H., 1993, Soil mechanics for unsaturated soils: John Wiley & Sons, New York.

Gassmann, F., 1951, Elastic waves through a packing of spheres: Geophysics, **16**, 673–685.

Hertz, H., 1882, On the contact of rigid elastic solids and on hardness, chapter 6: Assorted papers by H. Hertz: MacMillan, New York.

Ikari, M.J., and Kopf, A.J., 2011, Cohesive strength of clay-rich sediment: Geophysical Research Letters, **38**, L16309.

Ikelle, L., and Amundsen, L., 2005, Introduction to petroleum seismology: Society of Exploration Geophysicists, Tulsa, Oklahoma.

Krantz, R.W., 1991, Measurements of friction coefficients and cohesion for faulting and fault reactivation in laboratory models using sand and sand mixtures: Tectonophysics, **188**, 203–207.

Lu, N., and Likos, W.J., 2006, Suction stress characteristic curve for unsaturated soil: Journal of Geotechnical and Geoenvironmental Engineering, **132**, 131.

Lu, Z., and Sabatier, J.M., 2009, Effects of soil water potential and moisture content on sound speed: Soil Science Society of America Journal, **73**, 1614–1625.

Mavko, G., and Jizba, D., 1991, Estimating grain-scale fluid effects on velocity dispersion in rocks: Geophysics, **56**, 1940–1949.

Mavko, G., Mukerji, T., and Dvorkin, J., 2009, The rock physics handbook: Tools for seismic analysis of porous media: Cambridge University Press.

Mavko, G.M., and Nur, A., 1979, Wave attenuation in partially saturated rocks: Geophysics, **44**, 161–178.

Mindlin, R.D., 1949, Compliance of elastic bodies in contact: Journal of Applied Mechanics, **16**, 259–268.

Pham, H., Fredlund, D., and Barbour, S., 2005, A study of hysteresis models for soil-water characteristic curves: Canadian Geotechnical Journal, **42**, 1548–1568.

Rinaldi, M., and Casagli, N., 1999, Stability of streambanks formed in partially saturated soils and effects of negative pore water pressures: The Sieve River (Italy): Geomorphology, **26**, 253–277.

She, H.Y., and Sleep, B.E., 1998, The effect of temperature on capillary pressure-saturation relationships for air-water and perchloroethylene-water systems: Water Resources Research, **34**, 2587–2597.

Song, Y., Hwang, W., Jung, S., and Kim, T., 2012, A comparative study of suction stress between sand and silt under unsaturated conditions: Engineering Geology, **124**, 90–97.

Taylor, D.W., 1948, Fundamentals of soil mechanics: Soil Science, **66**, 161.

Terzaghi, K., 1943, Theoretical soil mechanics: John Wiley & Sons, New York.

Tinjum, J.M., Benson, C.H., and Blotz, L.R., 1997, Soil-water characteristic curves for compacted clays: Journal of Geotechnical and Geoenvironmental Engineering, **123**, 1060–1069.

Turner, J.S., 1979, Buoyancy effects in fluids: Cambridge University Press.

van Genuchten, M.T., 1980, A closed-form equation for predicting the hydraulic conductivity of unsaturated soils: Soil Science Society of America Journal, **44**, 892–898.

Velea, D., Shields, F.D., and Sabatier, J.M., 2000, Elastic wave velocities in partially saturated Ottawa sand: Soil Science Society of America Journal, **64**, 1226–1234.

Wulff, A.M., and Burkhardt, H., 1997, Dependence of seismic wave attenuations and velocities in rock on pore fluid properties: Physics and Chemistry of the Earth, **22**, 69–73.